



HAL
open science

Three-dimensional Monte Carlo study of three-terminal junctions based on InGaAs/InAlAs heterostructures

T. Sadi, F. Dessenne, Jean-Luc Thobel

► **To cite this version:**

T. Sadi, F. Dessenne, Jean-Luc Thobel. Three-dimensional Monte Carlo study of three-terminal junctions based on InGaAs/InAlAs heterostructures. *Journal of Applied Physics*, 2009, 105 (5), pp.0537075. 10.1063/1.3087703 . hal-00473651

HAL Id: hal-00473651

<https://hal.science/hal-00473651>

Submitted on 25 May 2022

HAL is a multi-disciplinary open access archive for the deposit and dissemination of scientific research documents, whether they are published or not. The documents may come from teaching and research institutions in France or abroad, or from public or private research centers.

L'archive ouverte pluridisciplinaire **HAL**, est destinée au dépôt et à la diffusion de documents scientifiques de niveau recherche, publiés ou non, émanant des établissements d'enseignement et de recherche français ou étrangers, des laboratoires publics ou privés.

Three-dimensional Monte Carlo study of three-terminal junctions based on InGaAs/InAlAs heterostructures

Cite as: J. Appl. Phys. **105**, 053707 (2009); <https://doi.org/10.1063/1.3087703>

Submitted: 06 December 2008 • Accepted: 19 January 2009 • Published Online: 05 March 2009

Toufik Sadi, François Dessenne and Jean-Luc Thobel



View Online



Export Citation

ARTICLES YOU MAY BE INTERESTED IN

[Analysis of the high-frequency performance of InGaAs/InAlAs nanojunctions using a three-dimensional Monte Carlo simulator](#)

Journal of Applied Physics **106**, 083709 (2009); <https://doi.org/10.1063/1.3248358>

[Empirical low-field mobility model for III-V compounds applicable in device simulation codes](#)

Journal of Applied Physics **87**, 2890 (2000); <https://doi.org/10.1063/1.372274>

[Semiconducting and other major properties of gallium arsenide](#)

Journal of Applied Physics **53**, R123 (1982); <https://doi.org/10.1063/1.331665>

Lock-in Amplifiers
up to 600 MHz



Zurich
Instruments



Three-dimensional Monte Carlo study of three-terminal junctions based on InGaAs/InAlAs heterostructures

Toufik Sadi,^{a)} François Dessenne, and Jean-Luc Thobel

l'Institut d'Electronique de Microélectronique et de Nanotechnologie (IEMN), UMR-CNRS 8520, 59652 Villeneuve d'Ascq Cédex, France

(Received 6 December 2008; accepted 19 January 2009; published online 5 March 2009)

We apply a three-dimensional (3D) semiclassical ensemble Monte Carlo simulation method to study T-branch junctions based on InGaAs/InAlAs heterostructures and obtain an accurate insight into the physics behind the operation of such structures. Electron transport in these devices is investigated and their rectifying behavior is demonstrated at 77 and 300 K and for different branch sizes. Detailed device analysis is performed to establish the relationship between the extent of ballistic transport and the rectifying behavior of the junctions and show the influence of surface charge effects, which are carefully included in the model. Results from the simulation of a T-branch junction with a Schottky gate terminal are presented, demonstrating the necessity of using 3D simulation models to study the physics of semiconductor junctions. © 2009 American Institute of Physics. [DOI: [10.1063/1.3087703](https://doi.org/10.1063/1.3087703)]

I. INTRODUCTION

The semiconductor device industry has witnessed a considerable growth in the past few decades relying mainly on device miniaturization to increase the packing density and hence the functionality of integrated circuits. However, with the device sizes reaching the nanometer range and the traditional scaling approaching its limits, innovative designs are needed to overcome these limits. The use of nanojunction devices based on III-As heterojunctions has been suggested as a possible solution for this problem. The amazing progress achieved in semiconductor heterostructure growth made the fabrication of such complex-geometry quasiballistic (low-scattering) nanodevices a possibility. They have attracted substantial attention in recent years due to their nonlinear properties, which are not observed in classical (diffusive) devices. This interest in nanojunctions is reflected by the significant number of publications presenting theoretical and experimental studies of such devices (e.g., Refs. 1–7). Examples of such structures studied in literature include four-terminal rectifiers,⁸ three-terminal junctions,³ and two-terminal ratchets.⁷

Initial III-As based junction devices have been fabricated using GaAs/AlGaAs heterojunctions.⁸ Improvements to these structures have been later achieved by using InGaAs channels with high indium (In) contents (>50%).⁹ The high electron velocity in such channels reduces the electron transit time, opening the possibility of using such devices, for example, for data processing at ultrahigh bit rate. Another important advantage discussed in literature is the compatibility of InGaAs-based ballistic devices with modern high electron mobility transistor (HEMT) technology. InGaAs-based HEMTs are already operational in the millimeter frequency range, and their integration with ballistic devices may result in extending the device operation to the terahertz regime.

This paper presents an analysis of the physics of three-terminal T-branch junctions (TBJs) by using a three-dimensional (3D) semiclassical ensemble Monte Carlo simulator. Three-terminal junctions are emerging devices that can be used for multiple purposes. Studies showed that the structures can function as voltage rectifiers,¹⁰ diodes,¹¹ and triodes¹² and can be incorporated as building blocks in electronic devices and circuits.¹³ The fundamental functioning of TBJs depends strongly on the improved electron transport in the junction. For this reason, TBJs are usually fabricated on high mobility heterostructures (as explained above) with the junction-region size being comparable to the mean free path of the two-dimensional electron gas (2DEG). Injected electrons entering the active region of the device do not lose their kinetic energy within this region, an observation which is at the origin of the rectifying behavior of a TBJ, as discussed later in this paper. The improved electron transport in the junction led to the common usage of the term “ballistic” to describe nanojunctions, although electron transport in the devices is not always purely ballistic. In fact, the rectifying behavior can be observed in junctions several times longer than the mean free path, in spite of the increased number of phonon interactions in these long devices.⁴ A pure ballistic behavior, where boundary scattering dominates, is only achievable with junction sizes of the order of the mean free path of electrons.

To the author's knowledge, only two-dimensional (2D) Monte Carlo models have been applied so far for the theoretical analysis of semiconductor nanojunctions (see, for example, Refs. 1, 3, and 6). An example of a very well-established 2D nanojunction simulation model is the one developed at the University of Salamanca.⁶ The application of this model involves performing 2D front-view simulations to account for the effect of the layer structure and 2D top-view simulations to account for the complex geometry of the device. The 2D nature of this model necessitates the use of a few nonphysical assumptions to generate the correct device

^{a)}Electronic mail: toufik.sadi@iemn.univ-lille1.fr. URL: <http://www.iemn.univ-lille1.fr>.

characteristics. As thoroughly explained in Ref. 6, the 2D model assigns a fixed average net doping to the channel obtained from front-view simulations. The effect of dopants is included when solving Poisson's equation to account for the effect of the fixed charge in the other layers. However, the model neglects the effect of impurity scattering caused by the presence of such dopants in the channel, a necessary assumption for good reproduction of transport effects, since the channel is supposed to be undoped (in reality). Although this very-well calibrated model may provide macroscopic results that are in very good agreement with experimental studies, the need for a very accurate study of electron transport at the microscopic scale, which is important in understanding the physics of these devices, requires the correct inclusion of the real device geometry in the 3D space.

This work presents a 3D analysis of electron transport in TBJs at low and room temperatures to provide a more accurate insight into their operation. Our model correctly includes the geometry of the simulated devices, which significantly minimizes the need for parameter fitting to match experimental results, and accurately accounts for electron transport effects. As well as extracting the macroscopic and microscopic characteristics of the simulated devices and demonstrating their rectifying behavior, the extent of ballistic transport is investigated in the structures. The influence of phonon and boundary scattering on the device characteristics is assessed and a relationship between ballistic transport and rectification in the devices is established. The objective of this work is also to discuss the importance of the 3D modeling of these heterojunction-based devices by presenting results from the study of advanced T-branch structures incorporating a Schottky gate terminal; in this part of the study, we demonstrate how the careful inclusion of the device geometry leads to more realistic macroscopic and microscopic characteristics.

II. SIMULATION MODEL

The Monte Carlo simulator self-consistently couples 3D electronic dynamics with a solution of the 3D Poisson's equation. This equation is solved using the finite difference scheme coupled with the cyclic Chebyshev method.¹⁴ Such iterative procedure is highly attractive in the solution of 3D Poisson's equation, as it allows a fast result convergence rate, and therefore a significantly minimized simulation time. A spherical nonparabolic band structure model of the materials of the layers forming the heterostructure (InAlAs and InGaAs) is used with electron transport taking place in the minima located at the Γ -, L -, and X -points of the Brillouin zone. All the important scattering processes are accurately accounted for in the simulation. These include intravalley electron-phonon scattering caused by acoustic and optical phonons, intervalley electron-phonon scattering, ionized impurity scattering, and alloy disorder scattering. Intravalley acoustic phonon scattering is treated as an inelastic process. The model also accounts for the effect of electron degeneracy. Two effects that are not usually considered in the simulation of nanojunctions are self-heating¹⁵ and hot phonons.¹⁶ Considering the lower biasing scheme employed

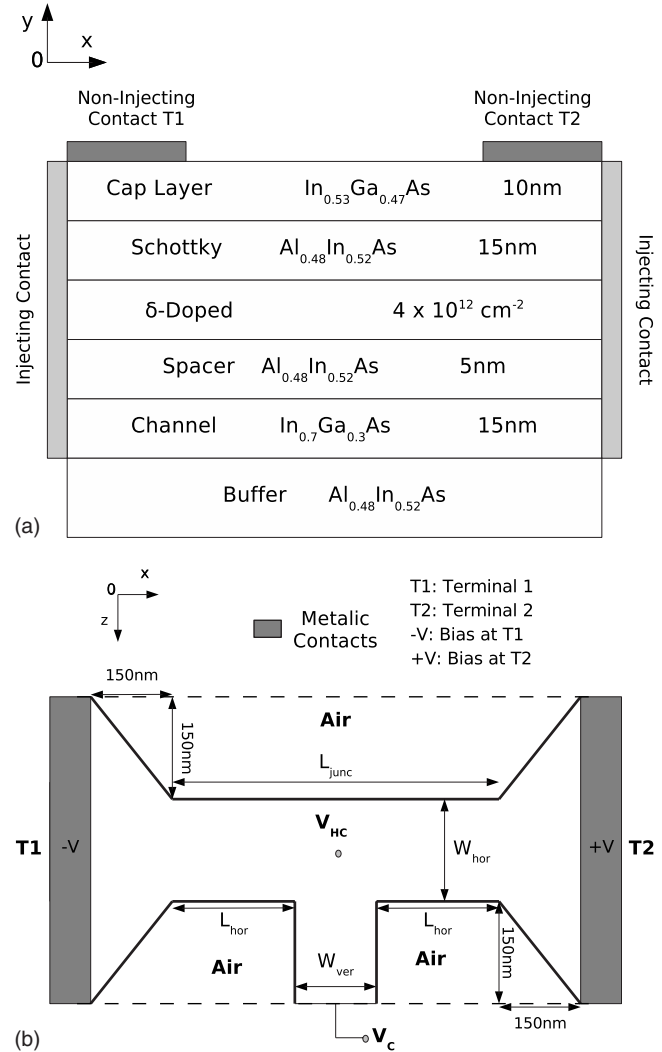


FIG. 1. 3D geometry and layer structure of the simulated TBJ. The (a) top figure shows a front view while the (b) bottom figure shows a top view of the simulated region of the device. All the semiconductor-air surfaces shown in (b) incorporate a surface charge (σ), adjustable using the algorithm described in Ref. 1. In (b), the variables W_{hor} and W_{ver} indicate the width of the horizontal and vertical branches, respectively, and L_{hor} indicates the length of the horizontal branch. L_{junc} indicates the total length of the junction. The figure also shows the domain in which Poisson's equation is solved, which includes an additional neighboring volume of air limited by the discontinuous border lines.

in these nanostructures to maintain the quasiballistic nature of transport, such effects may indeed be neglected. In this work, it is assumed that the phonon populations are at equilibrium with their occupation numbers being given by the Bose-Einstein distribution. The simulations are run assuming an isothermal temperature distribution equal to the ambient temperature (77 or 300 K), although the model can be readily extended to include self-heating.

The T-branch nanojunctions studied here are based on a δ -doped AlInAs/InGaAs heterostructure fabricated at the IEMN and described in Ref. 5. To illustrate how the geometry of the simulated devices is incorporated into the simulations, we show in Fig. 1 a front view and a top view of the simulated region of the T-branch nanojunction studied in this work, which is based on the structure studied in Ref. 1. The junction incorporates a main (horizontal) branch character-

ized by a width W_{hor} , a length L_{hor} , a total length L_{junc} , and a vertical branch characterized by a width W_{ver} . The Monte Carlo domain of simulation is limited to a small region of the device, which is in this case located between the two contact terminals (T_1 and T_2) at both sides of the main branch. Transport outside the simulated region is near equilibrium, and therefore uninteresting, but is time consuming to simulate because of the large charge densities involved. It is of note that such structure also incorporates a third terminal (T_3) located at the end of the vertical branch (see Ref. 5). In this part of the study, the device is biased in a push-pull fashion (as explained below), assuming an unbiased T_3 (i.e., with a floating potential). In this case, the bottom of the vertical branch is assumed to be open circuited. The rectifying behavior of the device is demonstrated by studying the variations in the output potential at the bottom end of this branch (V_C) and at the center of the main branch (V_{HC}) with the applied bias.

The simulation domain incorporates only a fraction of the top Ohmic contacts. Since the length of the simulated top Ohmic contact portions is much shorter than the real physical length of these contacts, most of the current flows into or out of the simulated region through the side boundaries (mainly in the channel) in the horizontal direction. Hence, the simulated top contact extensions are assumed to be noninjecting, as the vertical current flow through these contacts is negligible. Injecting contacts are introduced at both sides of the simulation domain just under the terminals to allow the injection of electrons into the simulated region using an algorithm that maintains an equilibrium Fermi–Dirac distribution at both boundaries.¹⁵

In this case, the electron densities in each layer are evaluated before running the Monte Carlo simulations by self-consistently solving a 2D Poisson's equation incorporating local densities obtained from the equilibrium Fermi–Dirac electron concentration relationship.¹⁷ Such model provides a realistic charge distribution at the injecting contacts without the need for parameter fitting, as used in 2D models which assume a fixed charge density along the contact determined from comparison with experimental results (see Ref. 6). The bias voltages at the top contacts are incorporated into the simulation by applying the Dirichlet condition at the area in the top surface of the device limited by the contacts. Since the junctions simulated here are characterized by a relatively high surface-to-volume ratio, the surface charge at the surrounding surfaces may significantly influence electron transport (see, for example, Refs. 1 and 18–20). The self-consistent charge model developed in Ref. 1 was implemented in our simulator to account for surface charge effects. Such model involves the dynamic adjustment of the surface charge according to the surrounding electron density. The surface charge at the free surfaces on top of the cap layer was set to a value of $5.0 \times 10^{12} \text{ cm}^{-2}$ to obtain good agreement with the experimental results presented in Ref. 1.

III. RESULTS, ANALYSIS, AND DISCUSSIONS

As mentioned earlier, the TBJs are biased in a push-pull fashion by applying a bias $-V$ at terminal T_1 and a bias $+V$ at

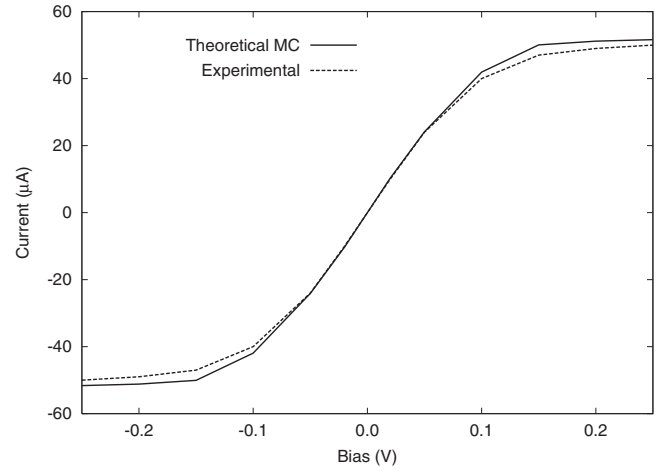


FIG. 2. Theoretical and experimental I - V characteristics of the TBJ with the following parameters: $W_{\text{hor}}=170 \text{ nm}$, $W_{\text{ver}}=60 \text{ nm}$, and $L_{\text{hor}}=250 \text{ nm}$. The results are obtained at room temperature (300 K).

terminal T_2 . This biasing scheme is suitable for the study of the rectifying behavior of the device, as discussed in literature.^{1,5,6,18,21} The reliability of our simulator has been validated by comparison with results obtained from the experimental study of similar nanojunction structures. To demonstrate the validity of our model, we show in Fig. 2 the I - V characteristics of the T-branch nanojunction shown above (obtained using our simulator) and the one studied in Ref. 1 (obtained experimentally) at room temperature. The device is characterized by the following parameters: $W_{\text{hor}}=170 \text{ nm}$, $W_{\text{ver}}=60 \text{ nm}$, and $L_{\text{hor}}=250 \text{ nm}$. As can be seen, excellent agreement with experimental results is obtained. The small discrepancies are not expected to affect the qualitative conclusions made in this work.

A. Analysis of TBJs at 300 K

In the following, unless specified otherwise, the simulations are run at room temperature (300 K) and the studied device is characterized by the following parameters: $W_{\text{hor}}=120 \text{ nm}$, $W_{\text{ver}}=60 \text{ nm}$, and $L_{\text{hor}}=150 \text{ nm}$. Figure 3 shows the variation in the normalized current I_N given by the ratio

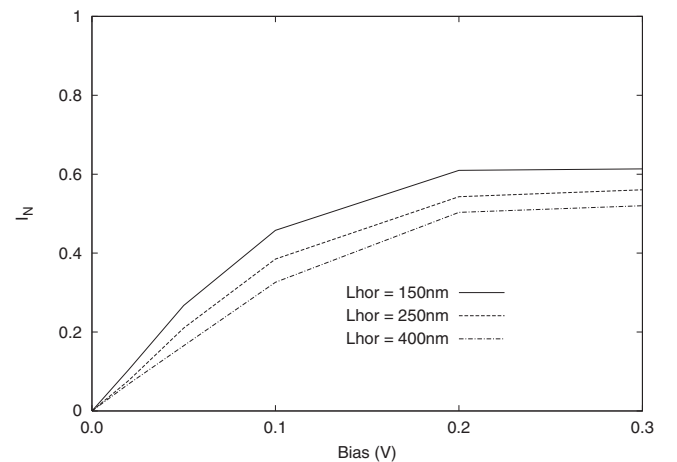


FIG. 3. Variation in the normalized current (I_N) with the applied bias (V) for a L_{hor} of 150, 250, and 400 nm.

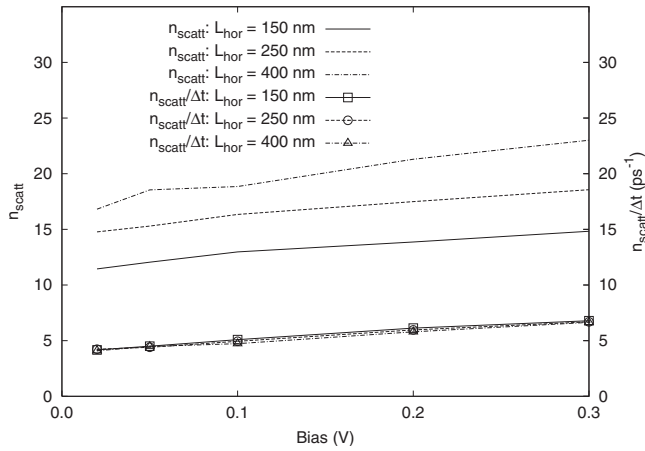


FIG. 4. Variation in n_{scatt} and $(n_{\text{scatt}}/\Delta t)$ with the applied bias (V) for a L_{hor} of 150, 250, and 400 nm.

of the saturation current to the total current injected by the contacts (see Ref. 6) with the bias V . Figure 4 shows the variation in the average number of scattering events per electron n_{scatt} in the simulation domain, which is assessed by considering only electrons who successfully travel from terminal T_1 to terminal T_2 . Figure 4 also shows the average number of scattering events per transition time (the average time Δt needed for an electron to travel from T_1 to T_2) in the simulation domain ($n_{\text{scatt}}/\Delta t$) as a function of V . The results in these figures are obtained for three different device sizes: for an L_{hor} of 150, 250, and 400 nm. Before starting the device analysis, it is important to establish the definition of the term ballistic frequently used to describe electron transport in nanojunctions. Traditionally, a device is referred to as ballistic when the influence electron scattering (via phonons, impurities, etc.) on transport is negligible compared to the influence boundary scattering. In practical terms, electron transport is referred to as ballistic, in this study, only when the average number of scattering events undergone by electrons in the junction is smaller than unity ($n_{\text{scatt}} < 1.0$). Considering the elevated n_{scatt} and the relatively low I_N , it is clear that the simulated TBJs are not “purely” ballistic at room temperature. Results at shorter horizontal branches show a lower n_{scatt} and a higher I_N , indicating an improvement in the extent of ballistic transport in the corresponding device. In spite of the visible difference in n_{scatt} , $(n_{\text{scatt}}/\Delta t)$ values are roughly the same in all three cases since the simulation are run at the same temperature (corresponding to the same mean free path).

Figure 5 shows the variation in V_C and V_{HC} with the bias V for the three L_{hor} values considered here. The coordinates at which the measurements of V_C and V_{HC} are taken are defined as follows. The x -coordinate (referred to as x_C) corresponds to the center of the vertical branch while the y -coordinate corresponds to the top interface of the channel (referred to as $y_{2\text{DEG}}$). In the case of V_{HC} , the z -coordinate (referred to as z_{HC}) corresponds to the center of the horizontal branch while in the case of V_C , the z -coordinate (referred to as z_C) corresponds to the bottom end of this branch (as indicated in Fig. 1). Figure 5 shows how V_C is not a faithful reflection of V_{HC} , as discussed in literature.¹ The higher

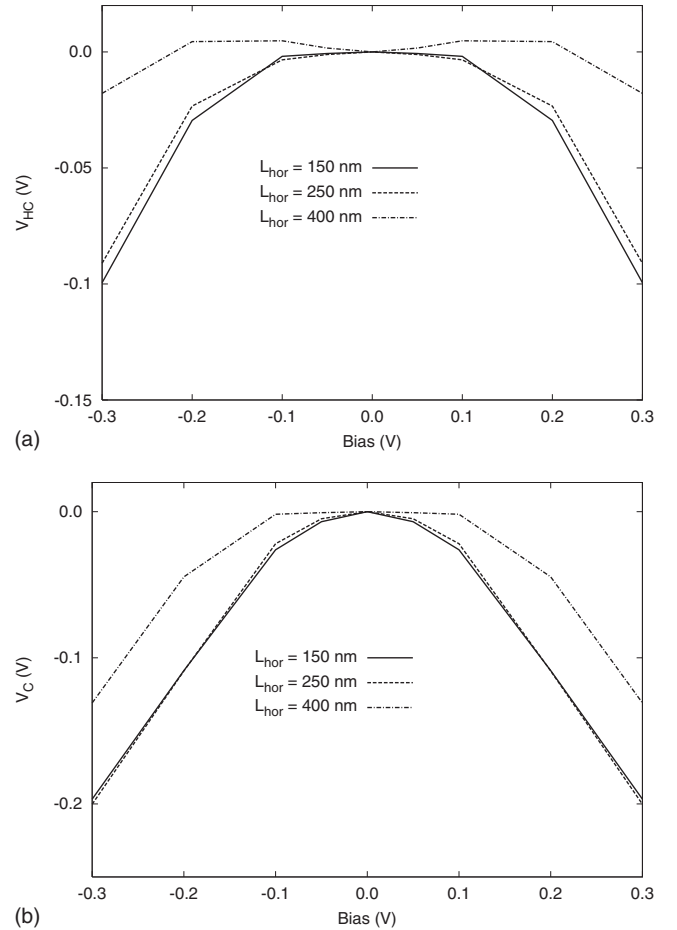


FIG. 5. Variation in (a) V_{HC} and (b) V_C with the applied bias (V) for a L_{hor} of 150, 250, and 400 nm.

negative values of V_C , as compared to that of V_{HC} for a given bias, is a direct consequence of the significant influence of the surface charge along the thin vertical branch. Such results demonstrate how surface charge plays an important role in defining the rectifying behavior of nanojunctions. More importantly, this example shows how the rectifying behavior can be observed even in long TBJs (with sizes several times longer than the mean free path), where transport is not purely ballistic.

Figure 6 shows the variation in the average electron density, velocity in the x direction, and kinetic energy in the channel at $z=z_{HC}$ at a given V for the three L_{hor} values. In general, the values of V_C and V_{HC} decrease at higher applied potentials due to the asymmetry in the mobile charge distribution in the device, as demonstrated in Fig. 6(a). Such effect, which is more pronounced at shorter (and hence more ballistic) devices, results from enhancing electron transport in the $+V$ terminal side of the junction, where electron velocity profiles demonstrate a strong peak value, as seen in Fig. 6(b). This behavior distinguishes nanojunctions from classical (diffusive) devices, where density and velocity profiles are expected to be symmetric, and V_{HC} , in this case, is not expected to vary significantly from 0 V. Figure 6(c) shows how electrons gain more energy in the junction region, an energy profile not observed in classical devices.

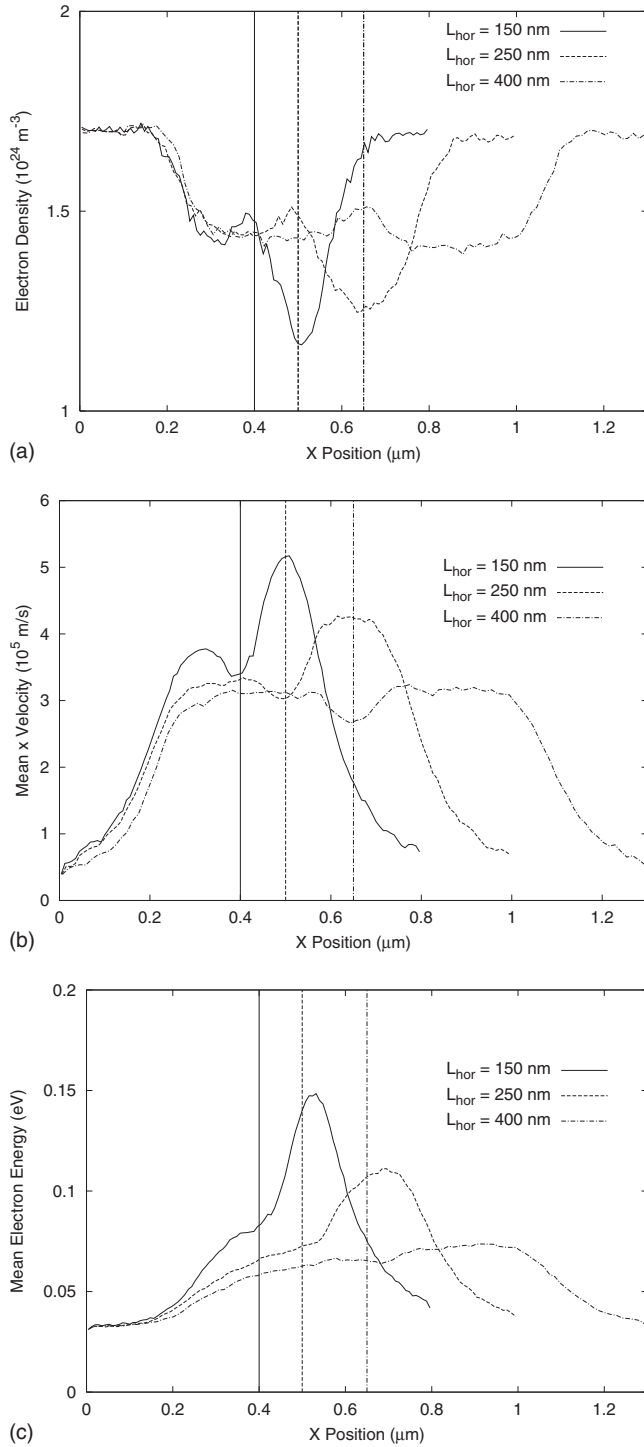


FIG. 6. (a) Variation in the mean electron density, (b) the velocity in the x direction, and (c) the electron kinetic energy in the channel at $z=z_{HC}$ for the three L_{hor} values. The results are obtained at a bias (V) of 0.2 V. The vertical lines shown in each figure indicate the x coordinate at the center of each junction ($x=x_C$) and are drawn with the same line style corresponding to each structure with a given L_{hor} .

Clearly, velocity overshoot is more important at shorter devices explaining the stronger variation in V_{HC} and V_C with the bias.

In a TBJ biased in a push-pull fashion, V_C can be described by a quadratic relationship $V_C \sim -\frac{1}{2}\alpha V^2$, where α is the curvature ($\alpha > 0$).⁴ The V_C curves shown in Fig. 5 can be divided into two regimes. In the central regime (at relatively

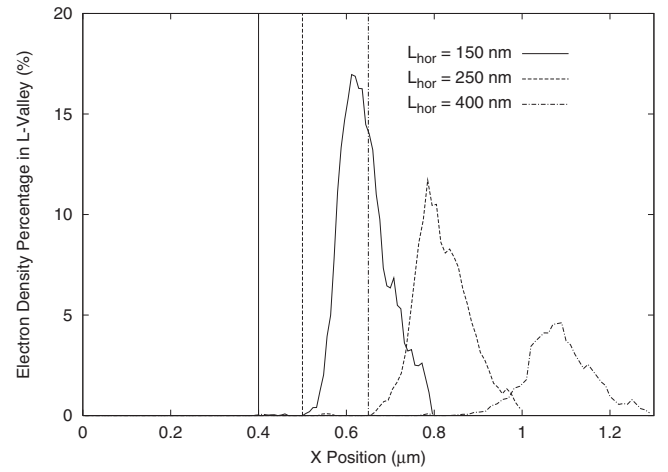


FIG. 7. The average electron density percentage in the L valley in the channel at $z=z_{HC}$ at a bias of 0.4 V for three L_{hor} values.

low V values), V_C decreases in a quadraticlike fashion, as described above, with the curvature α being generally higher at shorter devices. In the second regime (at higher V values), V_C decreases with increasing V in a near-linear fashion. It is of note that the maximum bias applied to such devices is carefully chosen, such that the effect of intervalley transitions does not adversely influence transport in the device. Figure 7, which shows the electron density percentage in the L valley in the channel at $z=z_{HC}$ at a high bias of 0.4V, demonstrates the strong increase in the number of intervalley transitions, directly resulting in reducing the average mobility of the 2DEG. Another effect of relative importance at relatively high biases is the transfer of electrons to the upper layers of the heterostructure, as illustrated in Fig. 8, which shows a 2D section of the electron distribution at $z=z_{HC}$ at the same bias and a L_{hor} value of 150 nm.

B. Influence of electron scattering on rectification

To analyze the relationship between the extent of ballistic transport and the rectifying behavior of the junction, we present in this section results from the study of the TBJ at different temperatures corresponding to different electron mean free paths. Figures 9 and 10 show the variation in I_N ,

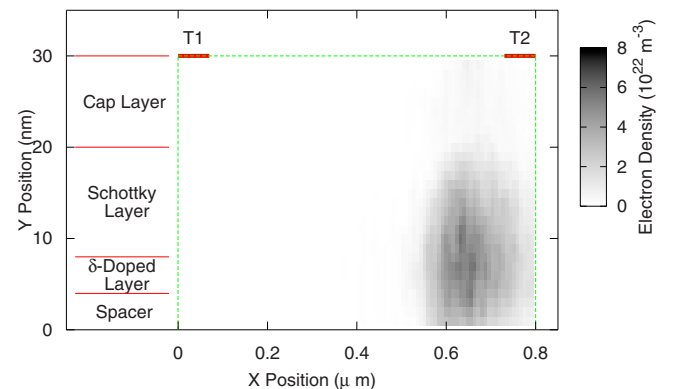


FIG. 8. (Color online) A 2D section of the electron density distribution at $z=z_{HC}$ and at a bias of 0.4 V and a L_{hor} value of 150 nm. In the y -axis, $y=0$ corresponds to the channel-spacer interface while $y=30$ nm represents the top surface of the device.

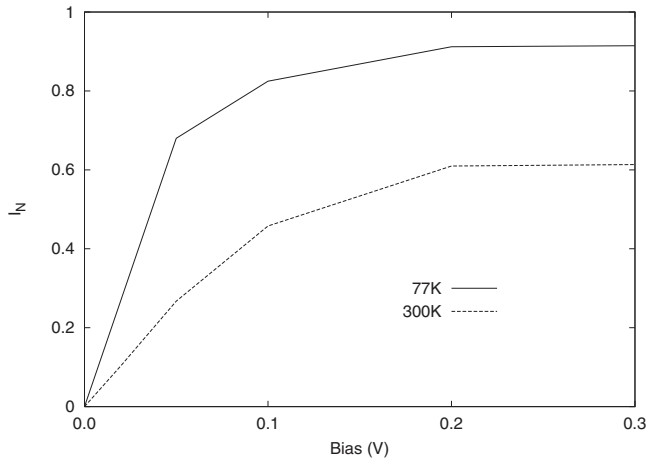


FIG. 9. Variation in the normalized current (I_N) with the applied bias (V) at 77 and 300 K for a L_{hor} of 150 nm.

n_{scatt} , and $n_{\text{scatt}}/\Delta t$, respectively, with the bias V at 77 and 300 K. As expected, results at 77 K show a reduced n_{scatt} and a relatively high I_N , corresponding to an improvement in the extent of ballistic transport in the device. However, the device is still not purely ballistic even at such a low temperature. While generally more negative values of V_C and a higher curvature are observed at 77 K, Fig. 11 shows an increase in V_{HC} at low biases before falling at relatively high biases. This observation can be explained by plotting the velocity, energy, and density profiles at $z=z_{HC}$, as shown in Fig. 12, at a low (0.1 V) and a high bias (0.3 V). The behavior at low biases is associated with the shift in the location of the maximum average velocity, and hence by current continuity the minimum electron density in the main branch to the negatively biased terminal side. Clearly, electrons are accelerated to a maximum average velocity before reaching the center of the device due to a reduced number of scattering events, a profile enhancing the behavior discussed above. At higher biases, a strong peak velocity is observed at the positively biased contact side, giving rise to a reduced V_{HC} . Figure 13 shows the average electron density percentage in the L valley in the channel at $z=z_{HC}$ at a bias of 0.4 V and for both temperatures. Clearly, electron transfer to the upper val-

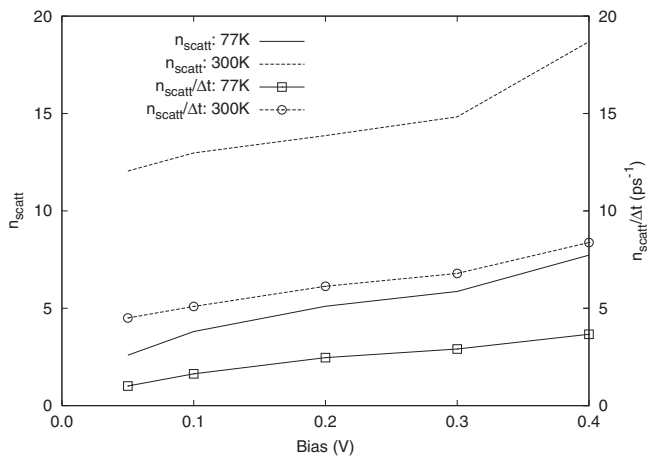


FIG. 10. Variation in n_{scatt} and $n_{\text{scatt}}/\Delta t$ with the applied bias (V) at 77 and 300 K for a L_{hor} of 150 nm.

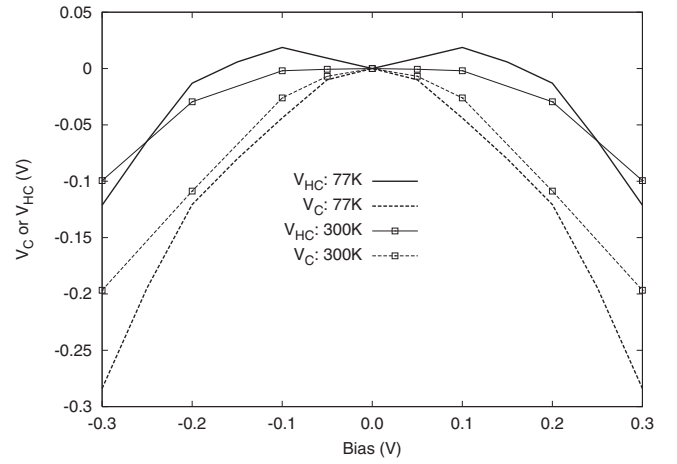


FIG. 11. Variation in V_C and V_{HC} with the applied bias (V) at 77 and 300 K for a L_{hor} of 150 nm.

leys is significantly enhanced at low temperatures, and therefore, the device bias should be kept to a minimum for the benefits of a high-mobility channel to be exploited at such temperatures.

Figure 14 shows the variation in the average net phonon emission density along the channel for both temperatures at a bias of 0.2 V. In spite of the reduced number of phonon scattering events at 77 K, more power dissipation is observed at such temperature, reflecting the increased current handling capability of the device at low temperatures. The reduction in the probability (P) of the phonon scattering mechanisms at low temperatures is directly due to the reduced phonon occupation number N . However, such reduction is also accompanied by a relative increase in the contribution of phonon emission events to phonon scattering [$P_{\text{ems}}\alpha(1+N)$] as compared to phonon absorption ($P_{\text{abs}}\alpha N$). Moreover, due to the reduced number of lattice interactions at 77 K, electrons are accelerated to higher peak energies, resulting in even more phonon emission events. Theoretically, in a truly ballistic device, the effect of electron scattering processes (mainly electron-phonon interactions) in the junction region is negligible compared to the effect of boundary scattering. However, as demonstrated in Fig. 14, phonon scattering still plays a significant role even at 77 K in the junction area of the device. Furthermore, the non-negligible power densities observed even at such low bias would suggest that self-heating may influence electron transport, an effect which is undesirable in quasiballistic devices.

C. Analysis of TBJs with a gate terminal

The purpose of introducing the 3D Monte Carlo simulator is to obtain a better idea about the operation of nanojunctions, which depends strongly on their complex geometrical shape in the 3D space, as well as to generate reliable results. While 2D models assume a fixed potential along the y -axis, our model accurately accounts for the variations in such quantity in the channel and in the whole simulated region. This allows the inclusion of some important physical effects such as electron transfer from the channel to other layers (see Fig. 8) and minimizes the need for parameter fitting (see, for

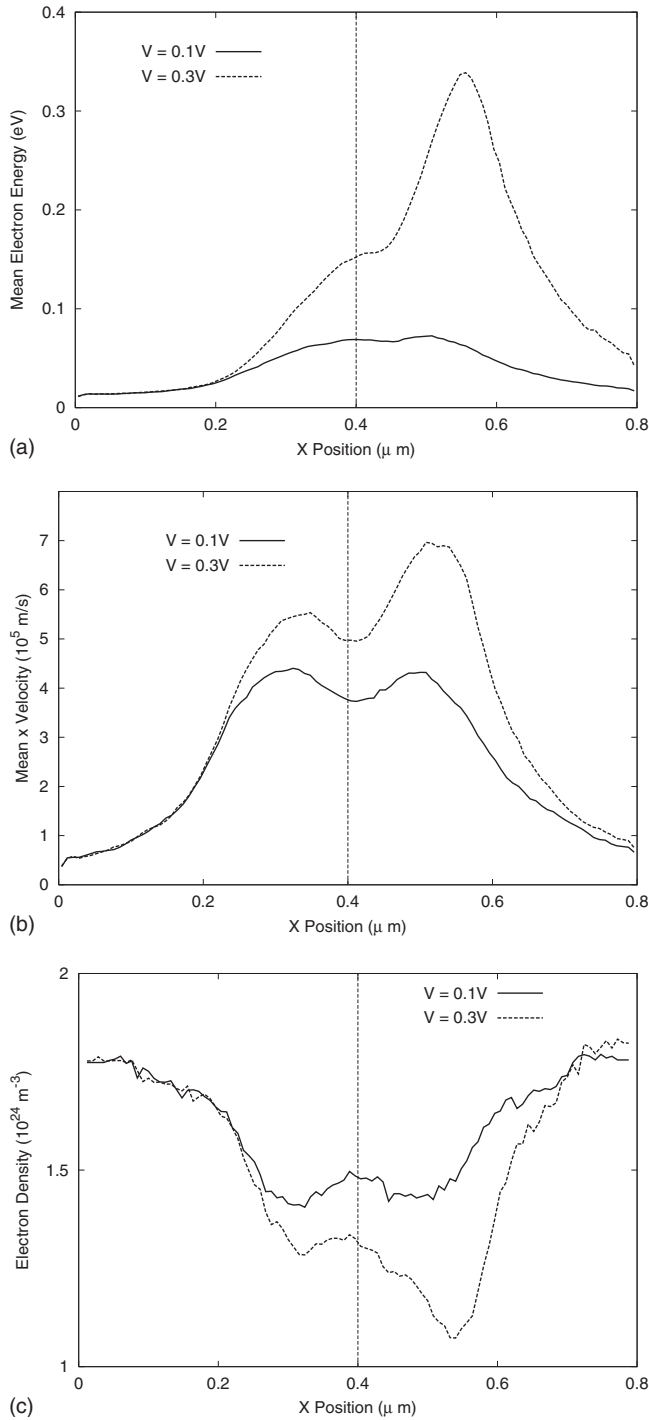


FIG. 12. (a) Variation in the mean electron energy, (b) the velocity in the x direction, and (c) the electron density at 77 K. The results are obtained at biases (V) of 0.1 and 0.3 V.

example, Refs. 1, 3, and 6) to generate the correct results. Most importantly, 3D models are necessary for the accurate modeling of structures where the electric field along the y -axis also plays a determining role in the device operation. An example of such structures is the three-terminal TBJ that incorporates a Schottky gate at the top surface.

In this part of the paper, we demonstrate the advantage of using our model by presenting results from the simulation of this structure. The gate electrode allows the junction to perform as a Multiplexer/Demultiplexer (MUX/DEMUX). In

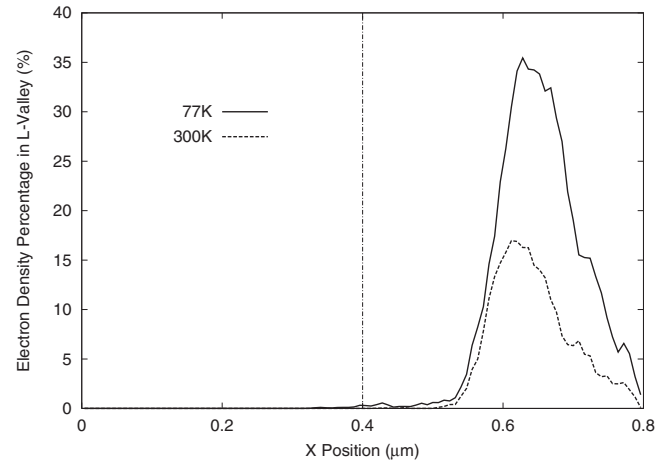


FIG. 13. The average electron density percentage in the L valley in the channel at the z coordinate, where V_{HC} is measured at 77 and 300 K for a bias of 0.4 V and a L_{hor} of 150 nm.

such a structure, which is shown in Fig. 15, current flow through contacts T_2 (I_2) and T_3 (I_3) is regulated by varying the gate potential (V_G). Two sets of results are generated: the first set is generated from the simulation of the real structure with a Schottky contact at the top surface, while the second set is generated assuming that the Schottky contact is located at the corresponding side surface (indicated in Fig. 15) as used in 2D simulations (see, for example, Ref. 6). The results include the variation in the currents flowing through the contacts as a function of the gate bias (shown in Fig. 16), density (shown in Fig. 17), and velocity in the x - and z -directions (shown in Figs. 18 and 19, respectively) in the channel at a

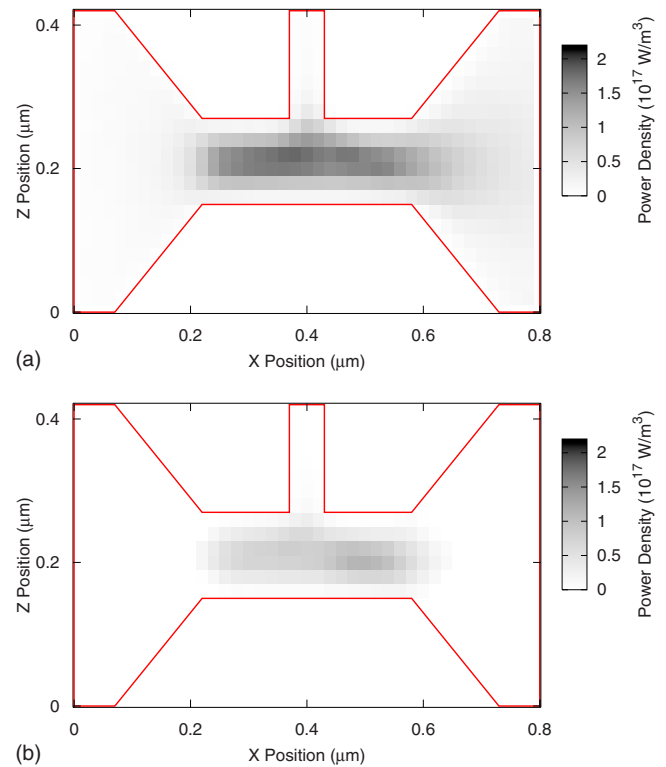


FIG. 14. (Color online) Variation in the average net phonon emission density along the channel at (a) 77 and (b) 300 K at a bias of 0.2 V.

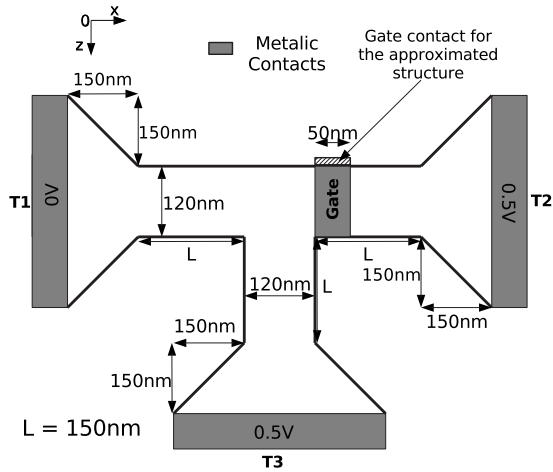
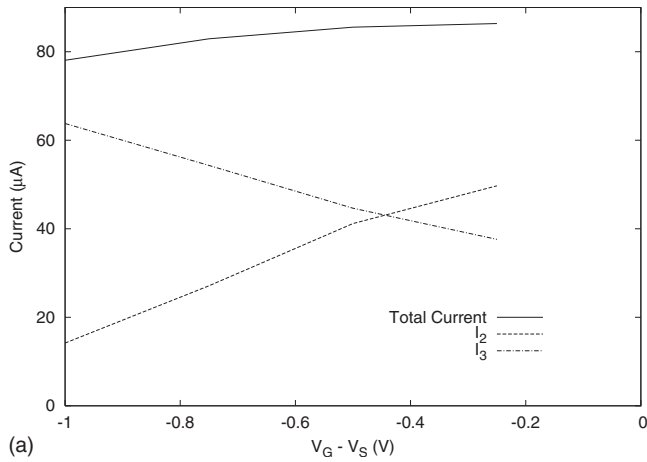


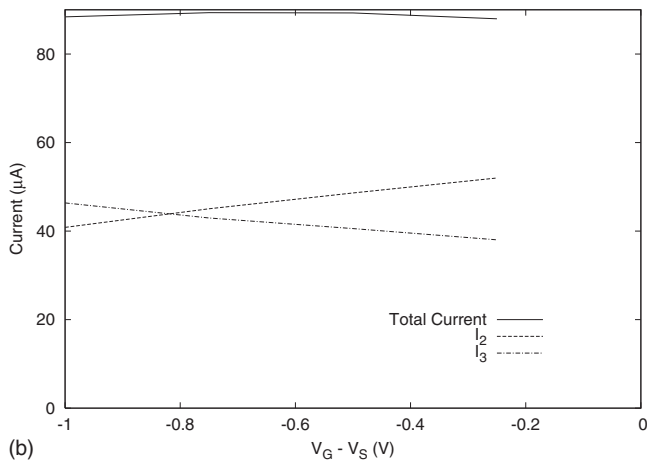
FIG. 15. 3D geometry and layer structure of the simulated TBJ with a gate contact.

given bias. For all gate biases, the potential values at T_1 (V_1), T_2 (V_2), and T_3 (V_3) are set to 0, 0.5, and 0.5 V, respectively.

Significant discrepancies in the current values are visible especially at lower gate biases, where the side-contact approximation leads to an overestimation of I_2 and an underestimation of I_3 . In this particular example, such approximation also results in a slight overestimation of the total current.

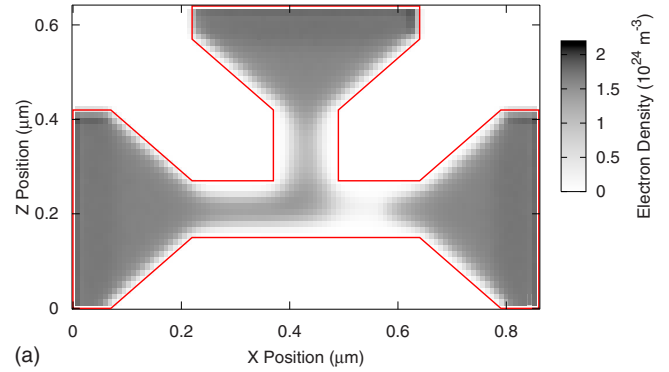


(a)

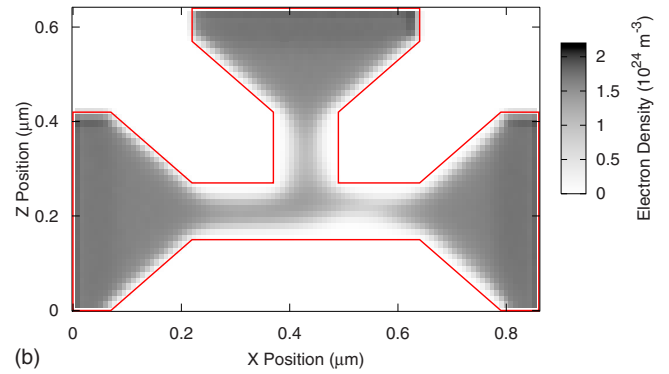


(b)

FIG. 16. The currents flowing through terminals T_1 , T_2 , and T_3 as a function of $(V_G - V_S)$, where V_S is the Schottky potential for (a) a top contact and (b) a side contact.



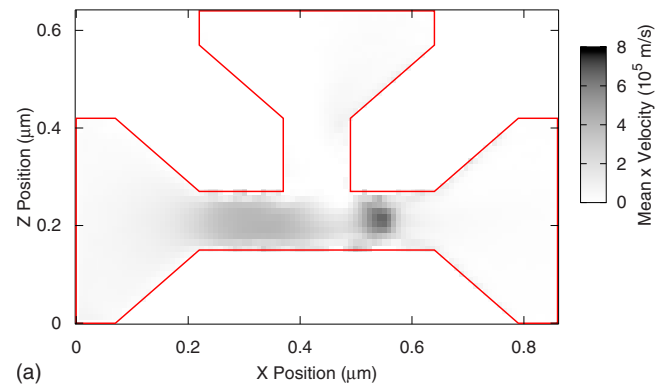
(a)



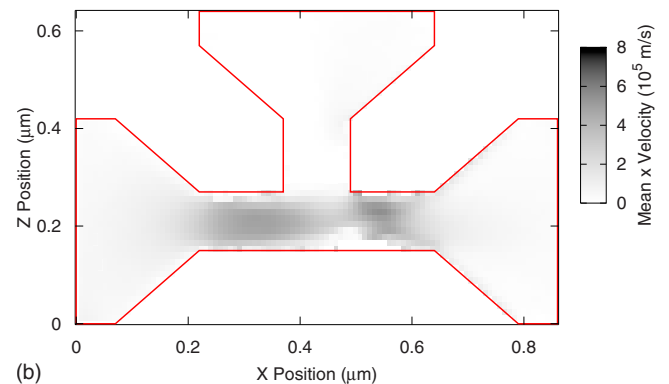
(b)

FIG. 17. (Color online) The distribution of electron density in the channel for (a) top and (b) side gate contacts at $V_G - V_S = -1.0$ V.

Moreover, the approximated structure gives an almost fixed total current, while in the real device such quantity increases slightly at less negative gate biases. This example demonstrates how the structure with a side gate is less efficient in



(a)



(b)

FIG. 18. (Color online) The variation in the velocity in the x direction for (a) top and (b) side gate contacts at $V_G - V_S = -1.0$ V.

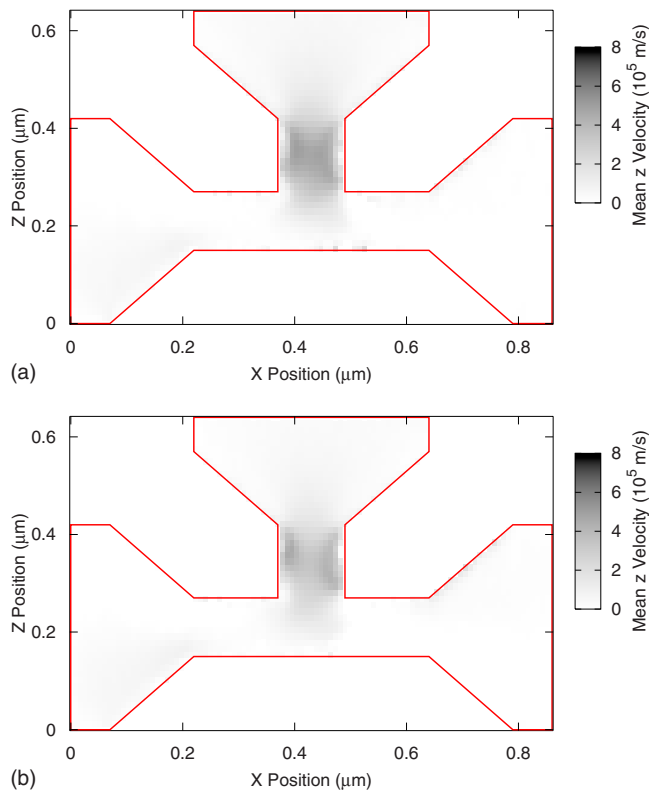


FIG. 19. (Color online) The variation in the velocity in the z direction for (a) top and (b) side gate contacts at $V_G - V_S = -1.0$ V.

regulating current flow in the junction. At the microscopic level, velocity and density profiles are also seriously affected by this approximation, as illustrated in Figs. 18, 19, and 17, respectively. Density profiles show that the device with a top gate contact gives a stronger electron depletion in the area around the gate, confirming the conclusion made above. Clearly, velocity profiles show stronger x and y velocity distributions (with higher peak values) in the case of a top gate contact. The work presented in this section is an example describing the case where the use of full 3D models is invaluable, since in this case 2D models can only reproduce some qualitative trends with less accurate results.

IV. CONCLUSION

This paper presents full analysis of TBJs using a 3D ensemble Monte Carlo simulator. The 3D model presented here is free from the approximations used in previously developed 2D models for the simulation of such structures, allowing an accurate qualitative and quantitative device study, both at the microscopic and macroscopic scales. In addition to discussing the advantages of 3D modeling and presenting the basic output characteristics of the devices, an analysis of the relationship between the rectifying behavior

of the device and the extent of ballistic transport in such structures was performed. The investigation of electron transport properties shows that the submicron devices simulated here are not purely ballistic since their sizes are several times longer than the mean free path. However, the potential values at the bottom of the central branch as a function of the applied bias demonstrate the improved nature of electron transport in the TBJ, an effect associated with space charge effects, as discussed above. This study concluded with the simulation of a MUX/DEMUX designed to take advantage of the benefits provided by TBJs, demonstrating the necessity of using 3D models for an accurate analysis of semiconductor junctions.

ACKNOWLEDGMENTS

The authors would like to thank Y. Roelens from the ANODE group (IEMN) for valuable discussions.

- ¹T. González, I. Iñiguez-de-la-Torre, D. Pardo, J. Mateos, S. Bollaert, Y. Roelens, and A. Cappy, *Phys. Status Solidi C* **5**, 94 (2008).
- ²S. Bollaert, A. Cappy, Y. Roelens, J. S. Galloo, C. Gardes, Z. Teukam, X. Wallart, J. Mateos, T. Gonzalez, B. G. Vasallo, B. Hackens, L. Berdnarz, and I. Huynen, *Thin Solid Films* **515**, 4321 (2007).
- ³L. Bednarz, Rashmi, P. Simon, I. Huynen, T. González, and J. Mateos, *IEEE Trans. Nanotechnol.* **5**, 750 (2006).
- ⁴D. Wallin, I. Shorubalko, H. Q. Xu, and A. Cappy, *Appl. Phys. Lett.* **89**, 092124 (2006).
- ⁵J. S. Galloo, E. Pichonat, Y. Roelens, S. Bollaert, X. Wallart, A. Cappy, J. Mateos, and T. González, Proceedings of the International Conference on Indium Phosphide and Related Materials, 2004 (unpublished), p. 378.
- ⁶J. Mateos, B. G. Vasallo, D. Pardo, T. González, J. S. Galloo, Y. Roelens, S. Bollaert, and A. Cappy, *Nanotechnology* **14**, 117 (2003).
- ⁷H. Linke, W. Sheng, A. Löfgren, H. Xu, P. Omling, and P. E. Lindelof, *Europhys. Lett.* **44**, 341 (1998).
- ⁸A. M. Song, A. Lorke, A. Kriele, J. P. Kotthaus, W. Wegscheider, and M. Bichler, *Phys. Rev. Lett.* **80**, 3831 (1998).
- ⁹A. M. Song, P. Omling, L. Samuelson, W. Seifert, I. Shorubalko, and H. Zirath, *Jpn. J. Appl. Phys., Part 2* **40**, L909 (2001).
- ¹⁰I. Shorubalko, H. Q. Xu, I. Maximov, P. Omling, L. Samuelson, and W. Seifert, *Appl. Phys. Lett.* **79**, 1384 (2001).
- ¹¹H. Q. Xu, *Appl. Phys. Lett.* **80**, 853 (2002).
- ¹²H. Q. Xu, I. Shorubalko, D. Wallin, I. Maximov, P. Omling, L. Samuelson, and W. Seifert, *IEEE Electron Device Lett.* **25**, 164 (2004).
- ¹³L. Worschech, D. Hartmann, S. Reitzenstein, and A. Forchel, *J. Phys.: Condens. Matter* **17**, R775 (2005).
- ¹⁴C. Jacoboni and P. Lugli, *The Monte Carlo Method for Semiconductor Simulation* (Springer-Verlag, Berlin, 1989).
- ¹⁵T. Sadi, R. Kelsall, and N. Pilgrim, *IEEE Trans. Electron Devices* **53**, 1768 (2006).
- ¹⁶T. Sadi and R. W. Kelsall, *IEEE Electron Device Lett.* **28**, 787 (2007).
- ¹⁷S. M. Sze, *Physics of Semiconductor Devices* (Wiley, New York, 1969).
- ¹⁸I. Iñiguez-de-la-Torre, J. Mateos, T. González, D. Pardo, J. S. Galloo, S. Bollaert, Y. Roelens, and A. Cappy, *Semicond. Sci. Technol.* **22**, 663 (2007).
- ¹⁹A. M. Song, M. Missous, P. Omling, I. Maximov, W. Seifert, and L. Samuelson, *Appl. Phys. Lett.* **86**, 042106 (2005).
- ²⁰J. Mateos, B. G. Vasallo, D. Pardo, and T. González, *Appl. Phys. Lett.* **86**, 212103 (2005).
- ²¹J. Mateos, B. G. Vasallo, D. Pardo, T. González, J. S. Galloo, S. Bollaert, Y. Roelens, and A. Cappy, *IEEE Trans. Electron Devices* **50**, 1897 (2003).